Inorganic Chemistry

pubs.acs.org/IC

Article

Donor Ability of Bisphosphinemonoxide Ligands Relevant to Late-Metal Olefin Polymerization Catalysis

Natalie S. Taylor, Maxwell T. Gordinier, Tejaskumar Suhagia, Danna D. Pinto, Demetrius D. Cherry, Dominic S. Verry, Lindsey N. Baker, Nathan J. DeYonker, Karin J. Young,* and Timothy P. Brewster*

Cite This: *Inorg. Chem.* 2024, 63, 2888−2898

Read Online

ACCESS | Metrics & More | Article Recommendations | Supporting Information

ABSTRACT: Late-transition-metal catalysts for polymerization of olefins have drawn a significant amount of attention owing to their ability to tolerate and incorporate polar comonomers. However, a systematic way to experimentally quantify the electronic properties of the ligands used in these systems has not been developed. Quantified ligand parameters will allow for the rational design of tailored polymerization catalysts, which would target specific polymer properties. We report a series of platinum complexes bearing bisphosphinemonoxide ligands, which resemble those used in the polymerization catalysts of Nozaki and Chen. Their electronic properties are investigated experimentally, and trends are rationalized by using computed spectral properties. Benchmarking computational data with known experimental parameters further enhances the utility of both methods for determining optimal ligands for catalytic application.

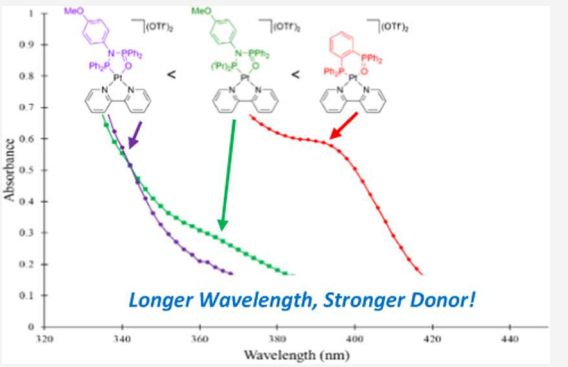

INTRODUCTION

Polymerization of olefins has long been a popular area of research, dating back to the development of the first commercial systems, the Ziegler−Natta system and the Phillips catalysts, in the 1950s and 1960s.[1,2] More than 20 million tons of polyolefin polymers are produced annually using these catalysts. However, polyolefins produced using these catalysts are typically nonpolar due to deleterious interactions between polar functionality and the early-metal active site, which puts some restrictions on their application.[3,4] Adding polar groups to the final polymer can improve important properties, such as printability and adhesion, and improve polymer affinity for fibers and pigments.[5−7] New designer catalysts have been sought to change the polymer properties and complement these industrial systems. Though not a fully solved problem, late-metal systems pioneered by, for example, Brookhart,[2,8−11] Drent,[6] Jordan,[12−14] Nozaki,[5,10,15,16] Chen,[17−20] and Carrow[21] have shown success in copolymerization of simple olefins with polar comonomers.[22−24] Most relevant to the work presented here, the Nozaki-type and Chen-type catalysts are comprised of a square planar palladium(II) center and chelating bisphosphinemonoxide (BPMO) ligands (Figure 1).

To improve upon current late-metal catalysts, it is important to understand the electronic factors within these systems and how they relate to the final polymer properties. In their initial report, Nozaki[15] and co-workers found that incorporating different R groups on the BPMO ligand led to different molecular weights and branching properties in the obtained polymers (Figure 1). It was found that incorporating electron-rich alkyl groups on phosphorus increased the polymer molecular weight and led to a higher degree of linearity when compared with the aryl analogue. Catalysts bearing ^{i}Pr and ^{t}Bu substituents were further used to copolymerize ethylene and polar vinyl monomers. Although a suggestion based on the polymerization data that strongly donating phosphines would improve the catalyst performance was made, there were no further experiments to explicitly measure or quantify ligand donor parameters for that system.

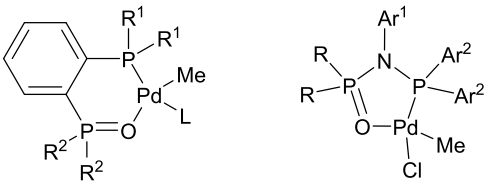

Figure 1. Palladium catalysts developed by Nozaki (left) and Chen (right). Nozaki: R^1 = ^{i}Pr, Ph; R^2 = Ph, ^{t}Bu, L = 2,6-dimethylpyridine Chen- R = Ph, Ar_2 = 2-methoxyphenyl.

Structure−function relationships are powerful tools for catalyst design. To this end, there have been numerous

Received: August 16, 2023
Revised: January 11, 2024
Accepted: January 12, 2024
Published: January 31, 2024

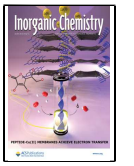

https://doi.org/10.1021/acs.inorgchem.3c02869
Inorg. Chem. 2024, 63, 2888−2898

attempts to develop universal metrics that can quantitate the steric and electronic properties of ligands. Most famous is the work of Tolman wherein he measured the donor properties of 70 phosphorus ligands bound to nickel tricarbonyl.[25] The derived Tolman electronic parameter (and related computational electronic parameter derived from DFT), based on the principle of carbonyl back-bonding, has been expanded to encompass a vast assortment of ligands and is now a standard offering in any introductory class in organometallic chemistry.[26,27] However, this system is best applied for monodentate phosphine ligands, not the BPMO ligands that are the targets of this study.

Other ligand parameters have been developed for targeted purposes. Our group recently published several papers in which the donor power of aluminum-containing ligands bound to late transition metals has been explicitly measured using carbonyl stretching frequency as the electronic probe.[28] A rhodium dicarbonyl fragment has been exploited by Crabtree et al. to measure the donor power of N-heterocyclic carbenes.[29] Ligand donor parameterization has also been explored in early-metal systems by Odom using a different methodology.[30] The work of Odom suggests that measurements of donor parameters are most useful when the system used to interrogate ligand properties is a mimic of that used in catalysis.

Ligand steric effects have also been extensively studied, with standard metrics such as percent buried volume, cone angle, and bite angle featuring prominently. The vast amount of experimental steric and electronic data available for simple ligands has led to the development of machine-learning-driven computational protocols, which can now be used to predict some ligand properties without the need for tedious synthesis.[31−33]

Most relevant to this work, there have been several attempts to develop a structure−function relationship between P−O ligands and the resulting catalytic activity in late-metal polymerization systems. Carrow related the activity of a series of BPMO ligands to percent buried volume and the CO stretch of a Rh(CO)Cl species in which the CO was located *trans* to the phosphine oxide/phosphoramide of interest. Mecking has found a strong correlation between phosphine donor power and polymer molecular weight in ethylene copolymerization, and Nozaki has found a relationship between ligand steric properties and polymerization outcomes in Drent-type phosphine sulfonate catalysts.[34,35] Nozaki and Sigman used statistical analysis to explore the catalytic performance of Drent-type phosphine sulfonate palladium catalysts for copolymerization.[36,37] Using machine learning, some components and parameters of a "useful" ligand were identified.[36] However, even with acknowledging these useful contributions, there is a need for *experimentally derived* ligand parameters. Additional metrics, which are easy to implement and provide reliable electronic information, can be used as both standalone predictors of catalyst behavior *and* incorporated into the workflow of machine learning systems to allow for better refinement.

Herein, we report a new system for electronically parameterizing ligands bound to platinum group metals. A drawback to the Vaska system studied previously by our group is that it is impractical for chelate ligands such as the BPMOs used in late-metal olefin polymerization catalysis. Thus, an alternative measure is required. Given that palladium(II) and nickel(II) systems are employed catalytically, we posited that electronic data generated from a platinum(II) analogue would provide an appropriate model. Specifically, we envisioned complexes of the type $[Pt(L)(bpy)]^{2+}$ (L = BPMO ligand, bpy = 2,2′-bipyridine; Figure 2) which are easily investigated via UV−vis

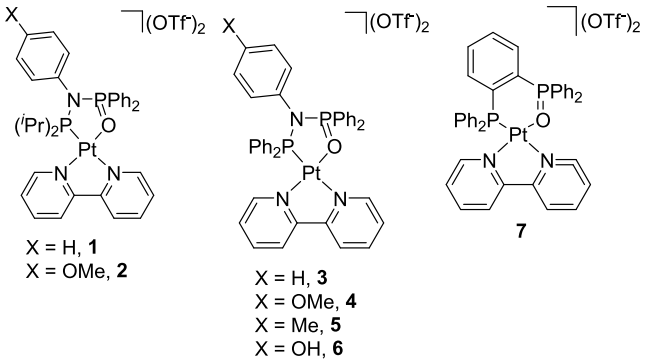

Figure 2. $[Pt(L)(bpy)]^{2+}$ complexes investigated in this study.

spectroscopy. The maximal energy of the low-energy $d \rightarrow \pi^*$ MLCT transition is known to be quite sensitive to the electronic nature of the supporting, nonbipyridine ligand.[38,39] We additionally hypothesized that chemical shift data from ^{195}Pt NMR spectroscopy would provide complementary electronic information regarding the donor ability of the BPMO ligands.[40] Though we were ultimately unable to obtain experimental ^{195}Pt NMR data for the complexes (see below), both absorbance data and NMR data have been modeled using density functional theory (DFT) methods to augment the experiment. We believe that our experimental evaluation of electronic parameters will complement the computational methods demonstrated in the literature[36] and allow for rapid experimental prescreening of potential chelate ligands for late-metal polymerization catalysts.

RESULTS AND DISCUSSION

Synthesis. Synthetic procedures for the desired $[Pt(bpy)L]^{2+}$ complexes **1**−**7** were adapted from the palladium catalyst syntheses of Chen[7] and Nozaki[15] (for full synthetic protocols, see the Experimental Details). Complexes **1**−**6** were obtained from 4-substituted anilines (Schemes 1 and 2). To obtain the desired BPMO ligands, the aniline derivatives were allowed to react with one equivalent of *n*-butyllithium (1.6 M in hexanes) followed by one equivalent of diphenylphosphinic chloride. Crude phosphoramide was obtained and used in the subsequent step after the removal of water-soluble byproducts. To obtain the BPMO, phosphoramide was allowed to react with *n*-butyllithium, (Scheme 1, step 2; Scheme 2, step 4) and then 1 equiv of the appropriate chlorophosphine. Filtration through a silica plug yielded crude BPMO as a white solid.

The final platinum complexes **1** and **2** (diisopropylphosphine) and **3**−**6** (diphenylphosphine) were obtained from the reaction of the crude BPMO and $Pt(bpy)Cl_2$.[41] AgOTf was utilized to facilitate the dissociation of chloride ligands. After workup, complexes **1**−**5** were obtained as yellow solids. Interestingly, after coordination with platinum, the MOM group is cleaved from the resulting platinum dication, yielding phenol complex **6**. Complex **6** is obtained as a pink solid.

Complex **7**, an analogue of the Nozaki catalyst,[15] was obtained through a similar reaction protocol (Scheme 3). Acetone was found to be a superior solvent to methylene chloride for this reaction, and celite filtration was found to

https://doi.org/10.1021/acs.inorgchem.3c02869
Inorg. Chem. 2024, 63, 2888−2898

Scheme 1. Syntheses of Complexes 1−5

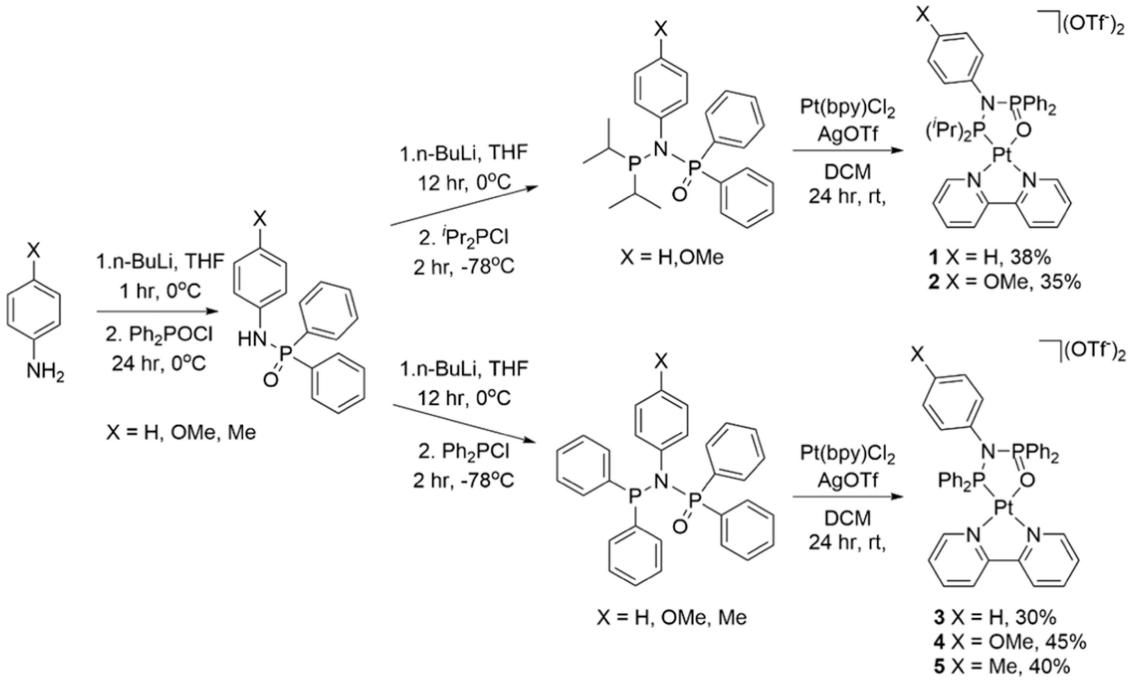

Scheme 2. Synthesis of 6

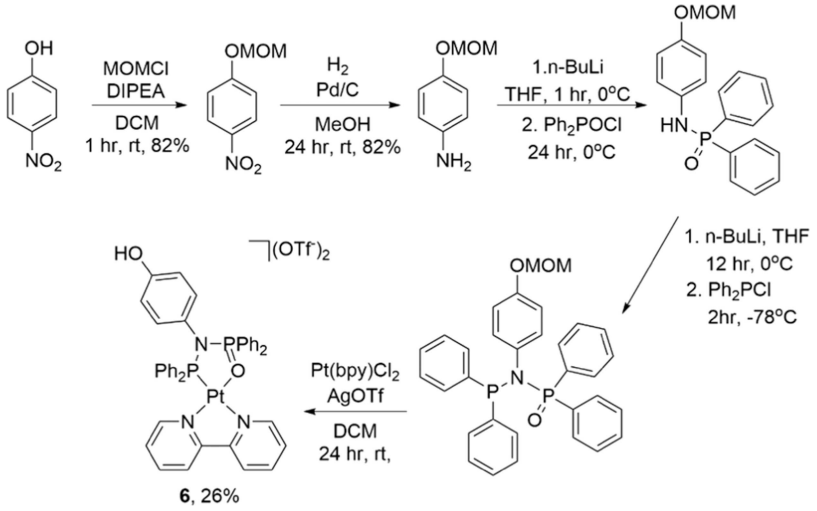

Scheme 3. Synthesis of 7

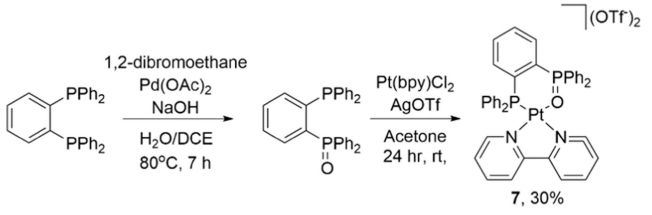

work well during workup (as opposed to silica; see the Experimental Details section). Interestingly, when filtration is attempted using a celite plug for **1** and **2**, it was noticed that the complexes decomposed.

Electronic Characterization. The value of complexes **1**−**7** derives from their ability to be utilized as electronic probes for ligand classes common to late-metal polymerization catalysis. As noted in the Introduction section, Pt^{II}(bpy)L complexes are well-known to undergo strong MLCT absorption under UV−vis irradiation. The absorbance maximum of the low-energy feature of the CT band has been previously shown to be dependent on the donor capacity of the supporting ligand.[38] Exploiting this knowledge, we conducted UV−vis absorbance experiments on all complexes to determine the donor abilities of our BPMO ligands. The spectral data can be found in Figures 3 and 4, and a tabulation of λ_{max} for the low-energy MLCT feature is provided in Table 1. Calculated extinction coefficients are consistent with a weak charge-transfer band and with computational data (see below). Plots of absorbance as a function of concentration for each complex can be found in the Supporting Information.

Careful analysis of the experimental data (column 2 in Table 1) suggests some noticeable trends. First, we will consider the effect of the R groups on the phosphine component of the

https://doi.org/10.1021/acs.inorgchem.3c02869
Inorg. Chem. 2024, 63, 2888−2898

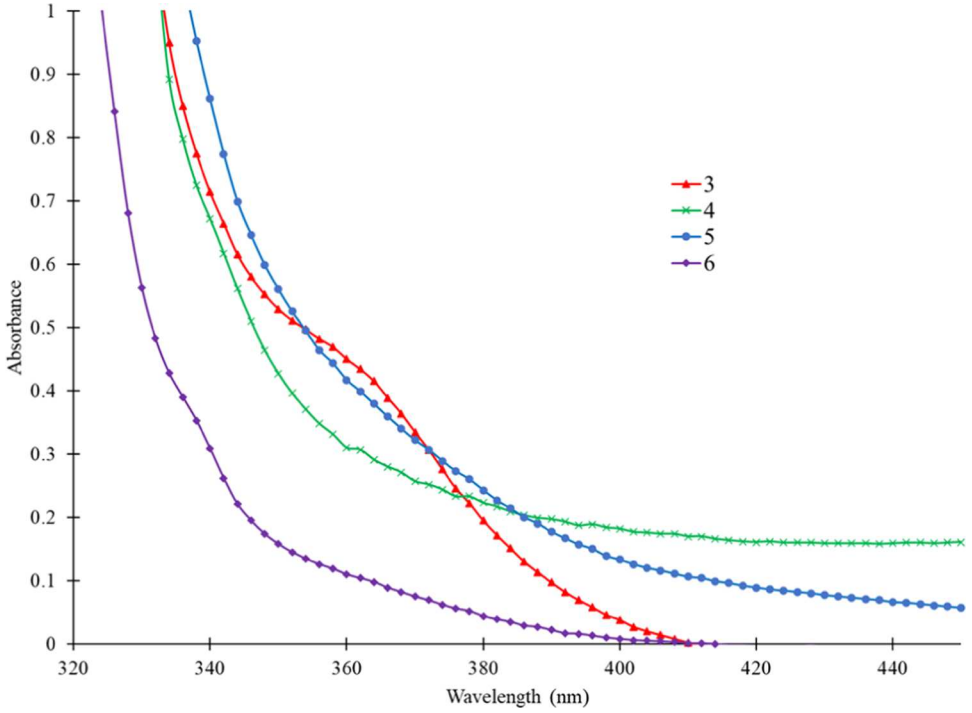

Figure 3. Truncated UV−vis spectra of complexes **3**−**6** in dichloromethane solution highlighting the lowest-energy MLCT transition.

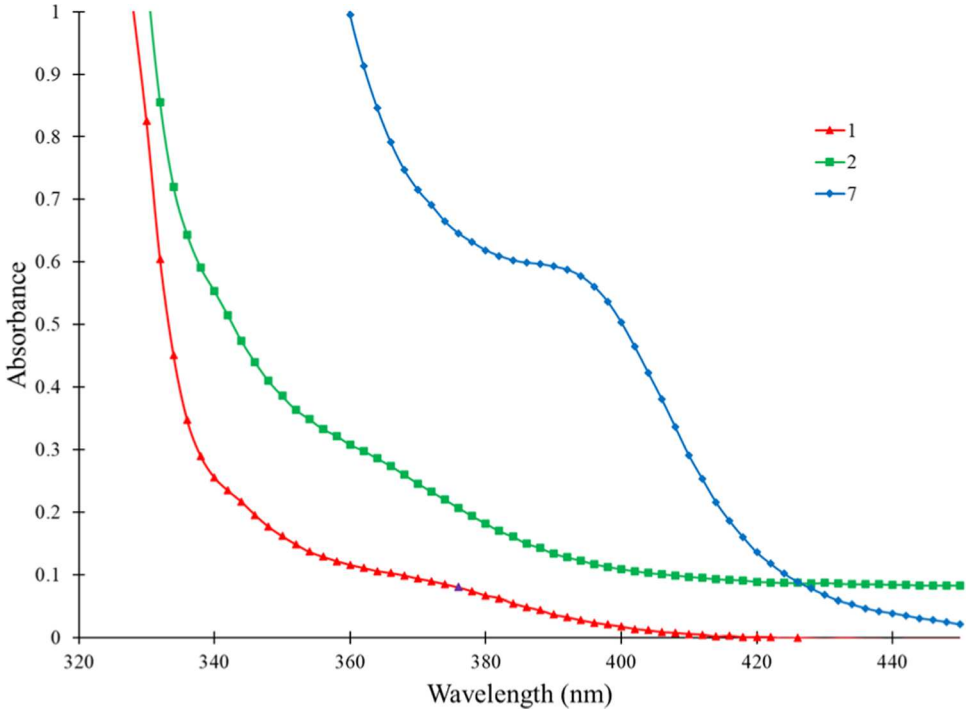

Figure 4. Truncated UV−vis spectra of complexes **1**, **2**, and **7** in dichloromethane solution highlighting the lowest-energy MLCT transition.

BPMO ligand. When comparing anisidine-derived complexes **2** and **4**, it is observed that λ_{max} hypsochromically shifts by 24 nm (600 cm^{-1}) on substitution of diisopropylphosphine with diphenylphosphine. A similar, though less dramatic, blue shift on changing from isopropyl substituents to phenyl substituents is seen for the aniline complexes **1** (370 nm, 27 000 cm^{-1}) and **3** (362 nm, 27 600 cm^{-1}). These data are consistent with the isopropyl phosphine serving as the stronger donor to the platinum center, as stronger ligand donors would be expected to absorb at lower energy due to destabilization of the occupied metal *d* orbital involved in the MLCT transition.[38,39] It is not surprising to find that diisopropylphosphine complexes **1** and **2** contain stronger donors than diphenylphosphine analogues **3** and **4**, as it has long been established that alkyl phosphines are stronger electron donors than aryl phosphines.

We also sought to understand the electronic effect of substitution of the aniline aryl ring in Chen-type catalysts. The

https://doi.org/10.1021/acs.inorgchem.3c02869
Inorg. Chem. 2024, 63, 2888−2898

Table 1. Tabulated Electronic Data for Complexes 1−7 in Dichloromethane Solution

complex	λ_{max} (nm, measured, ± 4)	λ_{max} (cm^{-1}, measured)	ε ($M^{-1}cm^{-1}$)	λ_{max} (nm, calculated)	$\lambda_{d,2}$ (nm, calculated)	^{195}Pt NMR chemical shift (ppm, calculated)
1	370	27 000	85	286.3	324.4	−3759
2	364	27 500	286	283.5	321.6	−3748
3	362	27 600	868	284.6	294.0	−3858
4	340	29 400	1344	284.6	294.7	−3845
5	364	27 400	379	284.3	294.7	−3843
6	336	29 800	780	284.3	294.1	−3864
7	394	25 400	1445	284.1	327.7	−3848

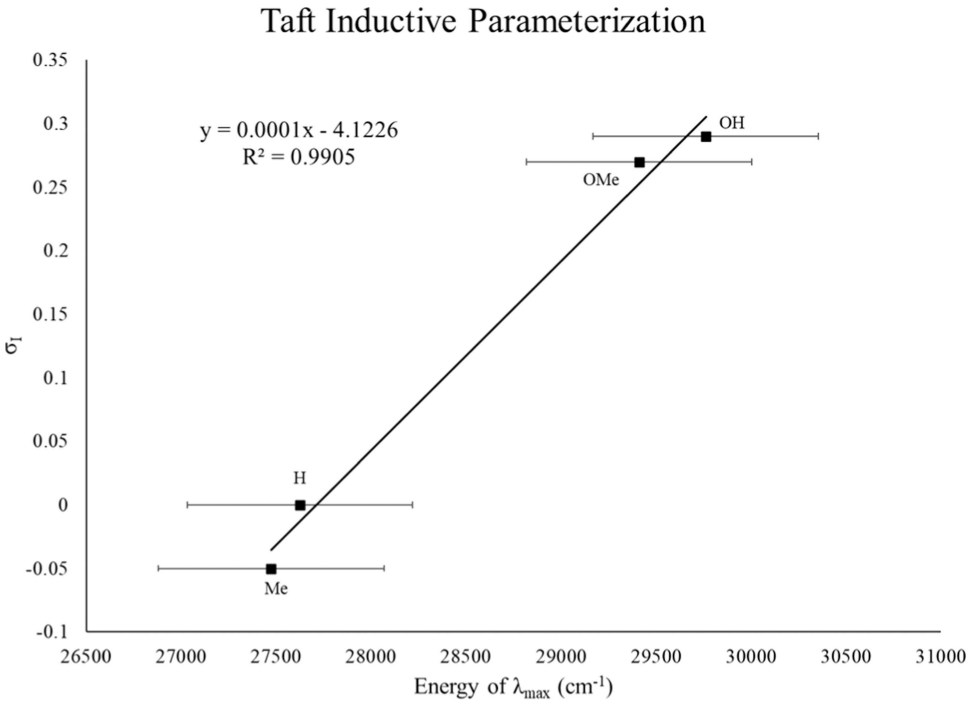

Figure 5. Correlation between σ_I and absorption energy of complexes **3**−**6**.

energies of the charge-transfer transitions for complexes **3**−**6** are 27 600, 29 400, 27 400, and 29 800 cm^{-1}, respectively. This indicates that absorption energy increases as R = Me < H < OMe < OH. As noted above, a higher-energy absorption is consistent with an electron-withdrawing effect due to stabilization of the occupied *d* orbitals at Pt.[38] These data are inconsistent with a resonance donor effect, as OMe and OH would be expected to be stronger donors than Me or H based on resonance. Unsurprisingly, a plot of observed absorption energies against the standard Hammett σ_p values yields a poor inverse correlation (see the Supporting Information). Structurally, this makes sense, as there is weak, if any, π-conjugation between the aniline ring and the phosphorus atom bound to the metal center. We, thus, hypothesized that inductive effects play the dominant role in determining the electron donor ability of the aniline ring. Gratifyingly, a plot of absorption energy against the Taft inductive parameter[42] (σ_I) yields a strong positive correlation (Figure 5). Substituents that are strongly inductively withdrawing (−OH, −OMe) yield the highest-energy transitions, as is expected.

The beauty of this electronic parameterization method is that it can be extended across platforms to draw comparisons between Chen-type[17] and Nozaki-type BPMO ligands.[15] UV−vis data show that the Nozaki ligand complex **7** possesses a lower-energy absorption feature than any of the Chen-type complexes **1**−**6**. This is consistent with the nitrogen bridge in the Chen-type BPMO framework serving as a relative electron-withdrawing functionality compared to the arene bridge in Nozaki-type complex **7**. Notably, both **2** and **7** contain phenyl rings appended to the phosphines, indicating that the difference in the bridging moiety must be responsible for the electronic change.

With a reliable experimental protocol in hand, we then sought to develop a computational model to support our experimental spectroscopic observations. We determined the electron donor ability of the ligands using two computational metrics: absorbance maxima derived from TD-DFT and calculated ^{195}Pt NMR chemical shifts.[40] Each calculated metric was then compared with the experimentally derived UV−vis absorption data to determine how well the calculated data correlated with the experiment. [NOTE: despite many attempts, experimental ^{195}Pt chemical shift data could not be obtained via either direct or indirect methods due to the fast quadrupolar relaxation of the Pt center by the strongly coupled ^{14}N atoms of the bipyridine ligand.]

Geometry optimizations of the various complexes were performed with ZORA-based DFT using the PBE0 functional (see the Synthetic Methods section). For all complexes discussed in this work, we discovered a surprising structural

https://doi.org/10.1021/acs.inorgchem.3c02869
Inorg. Chem. 2024, 63, 2888−2898

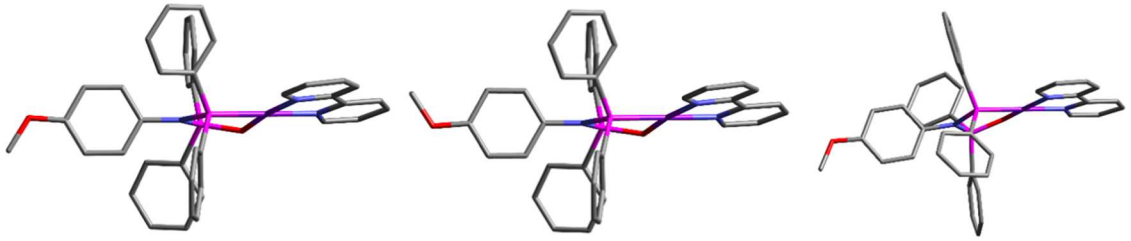

Figure 6. Three isoenergetic 3D structures of complex **4**. Hydrogen atoms are omitted for clarity. The left and middle structures are rotamers, with the OCH_3 group rotated by 180°.

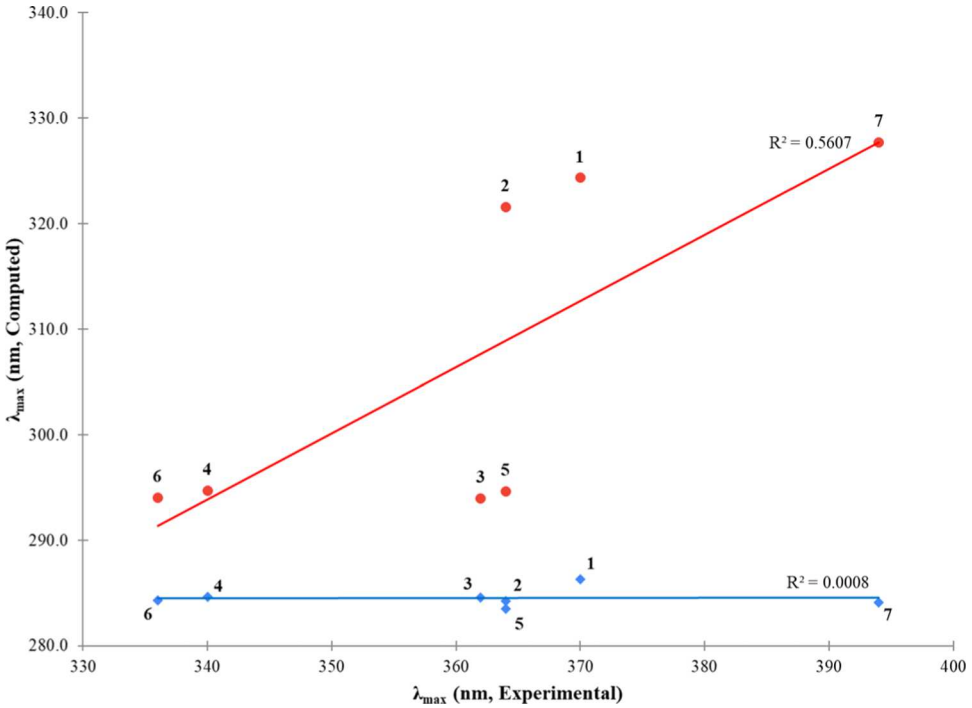

Figure 7. Comparison of theoretical UV−vis transitions with experimentally observed values (nm). Trend lines for λ_{max} (blue) and λ_{d_z2} (red) are plotted separately.

depth to the species due to the existence of energetically degenerate isomers arising from the conformational flexibility of the Pt−P−N−P−O metallacycle. Additionally, nearly degenerate hydroxy and methoxy rotamers of **2**, **4**, and **6** were located, and several local minima of **1** and **2** could be obtained depending on the coupled orientation of the two isopropyl groups. An illustrative example of the conformers considered for complex **4** is provided in Figure 6. With the exception of complex **6**, where one pair of the four structures is 1.0−1.1 kcal mol^{-1} higher in energy than the other pair, all isomers/rotamers of each complex are within 0.048 kcal mol^{-1} of the global minimum. To effectively correlate with experimental solution data, where degenerate conformers with a negligible barrier rapidly interchange, we considered the average calculated data of 2 isomers for complexes **1**, **3**, and **5** or an average of 4 structures (2 isomers x 2 rotamers) for complexes **2**, **4**, and **6**. Boltzmann averaging of the four structures of complex **6** produces nearly identical results to simple averaging of the UV−vis and chemical shift values in Table S1 (see the Supporting Information).

The right structure is a conformer of the middle structure arising from the inversion of the phosphorus and nitrogen centers. A fourth structure (not shown) is a rotamer of the right-side structure, with the OCH_3 group rotated by 180°. While the electronic energies of the four structures differ by only a maximum of 0.048 kcal/mol, the computed ^{195}Pt NMR chemical shifts range from −3854 to −3841 ppm.

We first compared computed UV−vis properties (TD-DFT simulated spectra for all complexes provided in Figure S1) to experimental data. We sought a correlation between two calculated values: transition energies corresponding to the singlet−singlet excitation with the largest oscillator strength above 280 nm (Figure 7, blue) and the singlet−singlet excitation corresponding to a transition dominated by the $5d_{z^2}$ occupied orbital (Figure 7, red) are listed in Table 1 (λ_{max} and λ_{d_z2} calculated, respectively). From the data in Figure 7 (blue), there is no correlation between the excitations selected by computed maximum oscillator strength energy values and the experimentally observed λ_{max}.

Next, wavelengths of transitions identified as originating from the occupied Pt $5d_{z^2}$ molecular orbital (λ_{d_z2} in Table 1) were plotted against experimental λ_{max} (Figure 7, red). This is the orbital transition that has been historically postulated to lead to the experimentally observed low-energy charge-transfer transition in complexes of the type $Pt(bpy)X_2$ (X = X-type ligand).[38] The computed λ_{d_z2} values of diisopropylphosphine

https://doi.org/10.1021/acs.inorgchem.3c02869
Inorg. Chem. 2024, 63, 2888−2898

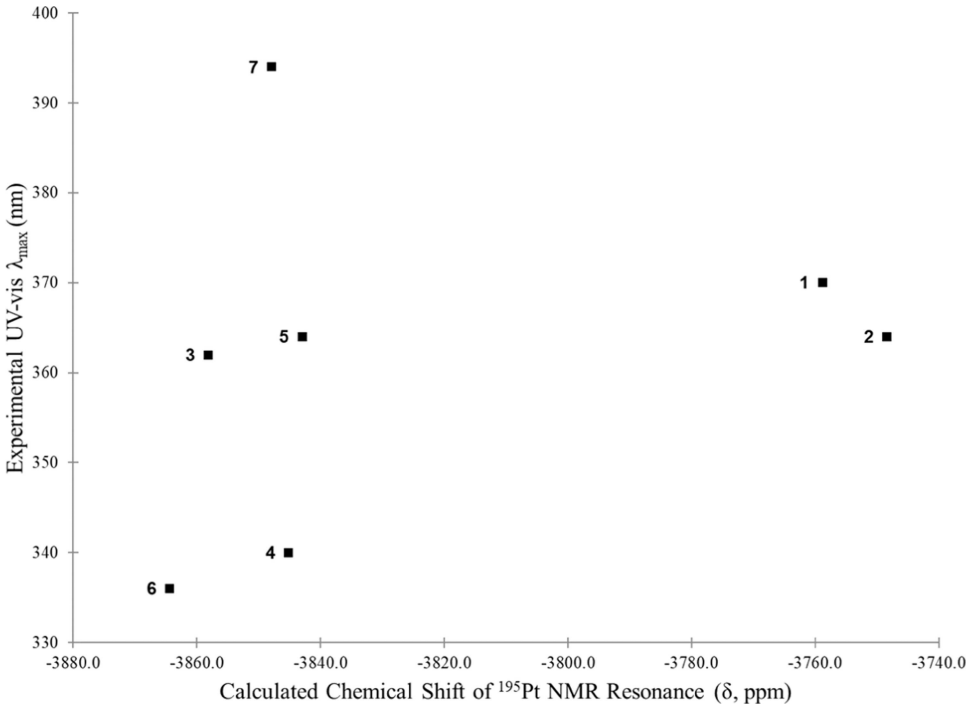

Figure 8. Comparison of calculated ^{195}Pt NMR chemical shifts with measured absorbance maxima.

complexes **1** and **2** are clustered between 320 and 324 nm, and transitions of complexes diphenylphosphine complexes **3**−**6** range from 294 to 295 nm, consistent with the experimentally observed blue shift on moving from isopropyl to phenyl substitution at the phosphine substituent. The overall correlation between the calculated energy of the $d \rightarrow \pi^*$ transition and the observed experimental absorbance energy is modest (R^2 = 0.56). There are two plausible reasons for this. First, as the $d \rightarrow \pi^*$ transition shifts to higher energy, it gets close in energy to the large charge-transfer feature present in all Pt(bpy)$^{2+}$ complexes. Accurate determination of λ_{max} is thus increasingly difficult as the donor ability of the BPMO ligand becomes weaker. Second, as the transition moves to higher energy, in the limiting case, it will cease to be the lowest-energy component of the experimentally observed shoulder. This is, notably, not an issue for strong donor ligands (complexes **1**, **2**, and **7** and Pt(bpy)X_2 complexes studied previously by Puddephatt)[38] where the $d \rightarrow \pi^*$ is further out in the visible region of the spectrum but can manifest more readily for very weakly donating ligands. These caveats do not cause us to doubt the validity of our parameter or the trends presented but serve as a reminder that this metric is not without limitations.

We then sought to establish whether an alternative computational metric, ^{195}Pt NMR shift, showed any correlation with experimental data. While a linear relationship may not necessarily be expected between the two measurements, ^{195}Pt chemical shifts are known to be highly sensitive to electronic changes in supporting ligands.[40] Our endeavor was immediately complicated by the conformational complexity of the BPMO ligands. Using ZORA defaults, calculated ^{195}Pt NMR chemical shifts for seemingly isoenergetic structures of a single complex were observed to differ by up to 110 ppm. Larger DFT integration grids (keyword DEFGRID) than those specified by default are necessary to compute accurate NMR properties for molecules with very heavy atoms like Pt. Calculated properly, differences in computed ^{195}Pt NMR chemical shift values show differences of 4−22 ppm. Though small, these differences in chemical shift values contribute some uncertainty to the correlation plot (Figure 8).

As can be seen, computed chemical shifts cluster for Chen-type complexes bearing phenyl substituents on the associated phosphines (**3**−**6**) and those bearing isopropyl substituents (**1**−**2**). This suggests that our employed computational methods are sufficient to distinguish between substituents bound to the phosphine moiety. There does not appear to be any useful correlation between the measured chemical shift and the identity of the X group bound to the aniline functionality, though it should be noted that the spans of calculated chemical shifts within complexes **1**−**6** are 12 and 21 ppm, respectively, which is likely within the experimental error of the calculation. Interestingly, the calculated NMR chemical shift for complex **7** is an outlier, grouping with complexes **3**−**6** rather than displaying the strong donor properties observed in the experimental UV−vis data. This result is also in direct contrast to the calculated $\lambda_{d_{z^2}}$, which tracks nicely with the experiment and predicts the Nozaki ligand to be a relatively strong donor. We do not yet know the reason for this discrepancy. Current studies are underway on a companion system for which ^{195}Pt NMR data can be obtained to determine if this observation extends to the experiment.

Overall, our results demonstrate that computational methods are sufficient for the accurate prediction of a ligand donor strength as a function of the R-group bond to phosphorus. We cannot make the same claim that computational methods accurately capture the experimentally observed effect of R-group substitution on the aniline backbone of complexes **1**−**6**. Conformational flexibility and the corresponding uncertainty imparted on computed data, particularly ^{195}Pt NMR chemical shifts, in the chosen model complex may prevent sufficient accuracy from being obtained to make these distinctions. We can, however, distinguish the electronic contribution of the aniline-bound functional groups exper-

https://doi.org/10.1021/acs.inorgchem.3c02869
Inorg. Chem. 2024, 63, 2888−2898

imentally, and a clear trend emerges that suggests that inductive effects are the dominant contributor to the electron donor power of the ligands.

CONCLUSIONS

In this report, we have established a simple method for experimentally quantifying ligand electronic effects in BPMO ligands. Our data support the logical conclusion that alkyl phosphines should serve as stronger electron donors to the metal center in BPMO complexes. Both experimental and computational data (UV−vis and ^{195}Pt NMR chemical shift) can readily distinguish between phosphine R substituents. Additionally, experimental data suggest that substituent effects on the aniline component in Chen-type BPMO ligands are inductive in nature, though this trend could not be modeled effectively computationally. This is likely due to the small range of calculated UV−vis absorption maxima and ^{195}Pt chemical shift data for each family of complex and the inherent conformational flexibility of the BPMO ligand framework adding uncertainty to the calculations. The larger calculated difference between complexes **1**−**6** in the chemical shift highlights the sensitivity of ^{195}Pt NMR to functional group changes and emphasizes the need to generate a companion system for which the ^{195}Pt NMR spectra can be reliably obtained experimentally. Work toward this goal, and the overall long-term goal of correlating measured donor parameters with polymerization data, is currently ongoing.

EXPERIMENTAL DETAILS

Synthetic Methods. Syntheses and manipulations were performed in a nitrogen-filled Inert Technologies glovebox or using standard Schlenk techniques unless otherwise specified. Deuterated solvents were purchased from Cambridge Isotope Laboratories, dried over molecular sieves or calcium hydride, and stored in a glovebox over molecular sieves prior to use. Dichloromethane, tetrahydrofuran, toluene, and pentane were dried on a Grubbs-type solvent purification system. Organic solvents were procured from commercial sources, dried using standard methods (Na, CaH) or on a Grubbs-type solvent purification system,[43] and stored in a nitrogen glovebox. All other reagents were purchased from commercial sources and used without further purification unless specified. Phosphine reagents were stored in a nitrogen glovebox prior to use. 1-(Methoxymethoxy)-4-nitrobenzene and 4-(methoxymethoxy)aniline were synthesized according to methods established in the literature.[44] 1,2-Bis-(diphenylphosphino)benzene monoxide (dppBzO) was synthesized according to methods established in the literature.[45] Procedures for ligand synthesis have been adapted from known methods of Chen and Nozaki[15,17] and can be found in the Supporting Information. ^{1}H, ^{13}C{^{1}H}, and ^{31}P{^{1}H} NMR spectra were recorded on a 400 MHz JEOL spectrometer and referenced to the residual solvent peak (^{1}H, ^{13}C{^{1}H}) or an external standard (^{31}P{^{1}H}). High-resolution mass spectra were recorded on a Waters SYNAPT quadrupole-time-of-flight instrument housed at the University of Memphis. Elemental analyses were conducted at the University of Memphis on a CE Elantech FlashSmart elemental analysis system. UV−vis data were recorded on a PerkinElmer Frontier FT-IR spectrometer in a dichloromethane solution.

General Procedure for Metalation of BPMO Ligands (Complexes 1 and 2). Under an inert atmosphere, Pt(bpy)Cl_2 (0.12 mmol) was added to a flask and dissolved in 25 mL of CH_2Cl_2. Silver triflate (0.23 mmol) was then dissolved in minimal CH_2Cl_2, added to the reaction, and stirred for 5 min. In a separate flask, the appropriate BPMO (0.12 mmol) was dissolved in 10 mL of CH_2Cl_2. The ligand solution was then added to the flask containing Pt(bpy)Cl_2 and silver triflate, and the mixture was stirred at room temperature for 24 h in the absence of light. The resulting suspension was filtered through a 0.22 μm syringe filter, and the solvent was removed in vacuo. The solid was then washed with hexane and diethyl ether to remove residual phosphine impurities. The complexes were then obtained as yellow solids. In some preparations, additional filtration is required to remove residual silver salts, as indicated by a darker color of the obtained solids. When needed, solids are redissolved in dichloromethane, passed through an additional syringe filter, and dried.

*[Pt(bpy)$_2$(N-(diisopropylphosphaneyl)-N,P,P-triphenylphosphinic Amide)][OTf]$_2$ (**1**).* (Yield: 0.042 g, 38%) ^{1}H NMR (400 MHz, acetone-d_6) δ 9.15−9.10 (m, 1H), 8.99 (d, J = 6.0 Hz, 1H), 8.88−8.79 (m, 2H), 8.62−8.55 (m, 2H), 8.02 (t, J = 6.6 Hz, 1H), 7.97−7.87 (m, 6H), 7.71 (dt, J = 8.0, 3.9 Hz, 4H), 7.65−7.53 (m, 2iH), 7.46 (t, J = 7.7 Hz, 2H), 7.09 (d, J = 7.9 Hz, 2H), 3.35−3.21 (m, 2H), 1.68 (dd, J = 20.3, 7.1 Hz, 6H), 1.18 (dd, J = 16.8, 6.9 Hz, 6H). ^{31}P NMR (162 MHz, acetone-d_6) δ 96.63 (d, J = 20.9 Hz), 67.01 (d, J = 20.8 Hz). ESI-MS calculated for [M-OTf]$^+$: 909.16, measured: 909.12. Elemental analysis: calculated: C 40.84, H 3.52, N 3.97; obtained: C 40.23, H 3.91, N 4.04.

*[Pt(bpy)$_2$(N-(diisopropylphosphaneyl)-N-(4-methoxyphenyl)-P,P-diphenylphosphinic Amide)][OTf]$_2$ (**2**).* (Yield: 0.035 g, 35%) ^{1}H NMR (400 MHz, acetone-d_6) δ 9.13 (td, J = 3.9, 1.9 Hz, 1H), 9.02−8.98 (m, 1H), 8.87−8.80 (m, 2H), 8.59 (tdd, J = 7.8, 6.2, 1.4 Hz, 2H), 8.06−8.00 (m, 1H), 7.98−7.88 (m, 6H), 7.77−7.68 (m, 4H), 7.51−7.43 (m, 1H), 6.97 (s, 4H), 3.80 (s, 3H), 3.25 (m, 2H), 1.67 (dd, J = 20.1, 7.1 Hz, 6H), 1.19 (dd, J = 16.7, 6.9 Hz, 6H). ^{31}P NMR (162 MHz, acetone-d_6) δ 71.59 (d, J = 33.8 Hz), 64.92 (d, J = 33.8 Hz). ESI-MS calculated for [M-OTf]$^+$: 939.17, measured: 940.13. Elemental analysis: calculated C 40.81, H 3.61, N 3.86; measured C 41.59, H 4.02, N 3.96.

*[Pt(bpy)$_2$(N-(diphenylphosphaneyl)-N,P,P-triphenylphosphinic Amide)][OTf]$_2$ (**3**).* (Yield: 0.35 g, 30%) ^{1}H NMR (400 MHz, acetone-d_6) δ 9.26 (ddd, J = 5.6, 4.1, 1.5 Hz, 1H), 8.84 (d, J = 8.0 Hz, 1H), 8.74 (dd, J = 8.1, 1.6 Hz, 1H), 8.62 (td, J = 7.9, 1.5 Hz, 1H), 8.39 (td, J = 7.9, 1.4 Hz, 1H), 8.26−8.17 (m, 4H), 8.12 (dd, J = 7.6, 5.8 Hz, 1H), 7.99−7.81 (m, 8H), 7.75−7.64 (m, 8H), 7.62−7.56 (m, 1H), 7.51−7.45 (m, 1H), 7.34 (td, J = 7.4, 6.8, 2.4 Hz, 1H), 7.12 (t, J = 7.9 Hz, 2H), 6.41 (dd, J = 8.5, 1.5 Hz, 2H). ^{31}P NMR (162 MHz, acetone-d_6) δ 96.08 (d, J = 24.0 Hz), 65.82 (d, J = 24.0 Hz). ESI-MS calculated for [M-OTf]$^+$: 977.82, measured: 978.12. Elemental analysis: calculated C 44.77, H 2.95, N 3.73; measured C 44.60, H 3.65, N 3.97.

*[Pt(bpy)$_2$(N-(diphenylphosphaneyl)-N-(4-methoxyphenyl)-P,P-diphenylphosphinic Amide)][OTf]$_2$ (**4**).* (Yield 0.055, 46%) 1H NMR (400 MHz, acetone-d6) δ 9.27−9.18 (m, 1H), 8.86−8.80 (m, 1H), 8.76−8.70 (m, 1H), 8.60 (td, J = 8.0, 1.6 Hz, 1H), 8.38 (td, J = 8.0, 1.4 Hz, 1H), 8.21 (ddd, J = 13.1, 8.5, 1.3 Hz, 4H), 8.12−8.04 (m, 2H), 7.99−7.88 (m, 6H), 7.87−7.82 (m, 2H), 7.74−7.65 (m, 9H), 7.48 (m, 1H), 7.40 (m, 1H), 6.63 (d, J = 9.1 Hz, 2H), 6.29 (d, J = 9.1 Hz, 2H), 3.67 (s, 3H).^{31}P NMR (162 MHz, acetone-d_6) δ 70.45 (d, J = 37.8 Hz), 64.88 (d, J = 37.8 Hz). ESI-MS calculated for [M-OTf]$^+$: 1007.84, measured: 1008.11. Elemental analysis: calculated C 44.64, H 3.05, N 3.63. Measured C 44.04, H 3.48, N 3.87.

*[Pt(bpy)$_2$(N-(diphenylphosphaneyl)-P,P-diphenyl-N-(p-tolyl)-phosphinic Amide)][OTf]$_2$ (**5**).* (Yield: 0.032g, 47%) ^{1}H NMR (400 MHz, chloroform-d) δ 8.94 (t, J = 4.9 Hz, 1H), 8.59 (d, J = 8.2 Hz, 1H), 8.49 (d, J = 8.1 Hz, 1H), 8.36−8.28 (m, 1H), 8.18−8.02 (m, 1H), 7.98 (dd, J = 13.2, 7.7 Hz, 4H), 7.82−7.68 (m, 8H), 7.58−7.68 (m, 10H), 7.33−7.18 (m, 1H overlapping with the solvent peak), 6.79 (d, J = 8.1 Hz, 2H), 6.02 (d, J = 8.0 Hz, 2H), 2.21 (s, 3H). ^{31}P NMR (162 MHz, acetone-d_6) δ 71.13 (d, J = 35.3 Hz), 64.68 (d, J = 35.4 Hz). ESI-MS calculated for [M-OTf]$^+$: 977.76, measured: 977.19. Calculated C 45.27, H 3.09, N 3.68. Measured C 48.00, H 4.02, N 3.33. This is consistent with 1 pentane of crystallization (C 47.53, H 3.91, N 3.46).

*[Pt(bpy)$_2$(N-(diphenylphosphaneyl)-N-(4-hydroxyphenyl)-P,P-diphenylphosphinic Amide)][OTf]$_2$ (**6**).* (Yield: 0.033 g, 26% of pink solid) ^{1}H NMR (400 MHz, acetone-$d6$) δ 9.25 (td, J = 4.8, 4.0, 1.5 Hz, 1H), 8.84 (d, J = 8.2 Hz, 1H), 8.74 (dd, J = 8.2, 1.5 Hz, 1H), 8.62 (td, J = 7.9, 1.5 Hz, 1H), 8.40 (td, J = 7.9, 1.4 Hz, 1H), 8.32 (dd, J =

https://doi.org/10.1021/acs.inorgchem.3c02869
Inorg. Chem. 2024, 63, 2888−2898

6.4, 3.0 Hz, 1H), 8.26−8.16 (m, 4H), 8.15−8.09 (m, 1H), 7.99−7.87 (m, 6H), 7.87−7.81 (m, 1H), 7.70 (qd, J = 8.0, 3.8 Hz, 8H), 7.53−7.45 (m, 2H), 6.53 (d, J = 8.9 Hz, 2H), 6.21−6.14 (m, 2H). ^{31}P NMR (162 MHz, acetone-d_6) δ 70.20 (d, J = 38.7 Hz), 64.57 (d, J = 38.8 Hz). ESI-MS calculated for $[M\text{-}OTf]^+$: 993.81, Measured: 993.08. Elemental analysis: calculated: C 44.14, H 2.91, N 3.68; Measured C 44.55, H 3.43, N 4.00.

[Pt(bpy)(dppBzO)](OTf)$_2$ (7). Pt(bpy)Cl$_2$ (100 mg, 1 equiv) was dissolved in 15 mL of acetone, and the solution was sparged with nitrogen. In a separate container, AgOTf (122 mg, 2 equiv) dissolved in 10 mL of acetone was sparged with nitrogen, and then the solution was added to the Pt(bpy)Cl$_2$ suspension. In a separate container, dppBzO (102 mg, 1 equiv) was dissolved in 15 mL of acetone and added to the mixture of Pt(bpy)Cl$_2$ and AgOTf. The reaction vessel was wrapped in foil to protect from light and heated to reflux for 2 h. The reaction mixture was filtered over celite to remove AgCl, and the pale yellow solution was evaporated to dryness to give a yellow solid. Further purification to remove phosphine impurities was achieved by washing the solid with hexane and diethyl ether (yield: 0.080 g, 30%) ^{1}H NMR (400 MHz, acetone-d_6) δ 9.21 (t, J = 4.9 Hz, 1H), 8.82 (d, J = 8.2 Hz, 1H), 8.68 (d, J = 8.2 Hz, 1H), 8.61 (t, J = 8.0 Hz, 1H), 8.31 (t, J = 7.9 Hz, 1H), 8.12 (t, J = 6.4 Hz, 1H), 8.07 (t, J = 7.2 Hz, 1H) 7.96 (dd, J = 13.3, 7.8 Hz, 6H), 7.87−7.92 (m, 1H), 7.78 (t, J = 7.7 Hz, 2H), 7.67 (dd, J = 13.3, 7.6 Hz, 6H), 7.52 (m, 9H) 7.25 (t, J = 8.0 Hz, 1H). ^{31}P NMR (162 MHz, acetone-d_6) δ 53.73 (d, J = 20.2 Hz), 2.29 (d, J = 20.4 Hz). ESI-MS $[m/z]^+$ calculated for $[M\text{-}OTf]^+$: 962.81, measured: 962.03. Elemental analysis: calculated C 45.37, H 2.90, N 2.52; measured C 46.61, H 3.39, N 2.49. This is consistent with one associated diethyl ether molecule (C 46.59, H 3.57, N 2.36).

Method for Obtaining UV−Vis Data for Complexes 1−7. UV−vis data were recorded in dichloromethane solution across a concentration range from 0.125 to 1 mM. Data were recorded using a 1 cm glass cuvette stoppered with a septum to prevent air from entering the sample during analysis.

Computational Methods. The electronic structure of the investigated complexes was executed utilizing density functional theory (DFT) with the PBE0[46,47] functional and an atom-pairwise dispersion correction via the Becke−Johnson damping scheme (D3BJ).[48,49] All computations were performed using the ORCA software package (version 5.0.4).[50] The ZORA-TZVP basis sets were employed for H, C, N, O, and P atoms, while the SARC-ZORA-TZVP basis sets were utilized for the Pt atom.[51,52] To account for relativistic effects in the geometry optimizations and calculation of NMR chemical shifts, the zero-order regular approximation (ZORA) methodology was implemented.[53−55] The gauge-including atomic orbital (GIAO) scheme has been utilized in the calculations of ^{195}Pt NMR chemical shifts to ensure the gauge-independent condition.[56,57] Analytical calculation of the Hessian matrix for the optimized structures confirmed the presence of appropriate minima (the absence of imaginary harmonic vibrational frequencies). A hybrid approach incorporating the resolution of identity and chain of sphere exchange algorithms (RIJCOSX) was applied[58] to reduce computational effort. Self-consistent field (SCF) calculations were tightly converged (keyword = TightSCF). A large DFT integration grid size (keyword = DefGrid3) was necessary to obtain reliable ^{195}Pt NMR chemical shifts. Solvent effects in the computations were considered using the conductor polarizable continuum model (CPCM).[59] The dichloromethane solvent parameters were used and characterized by a dielectric constant (ε) of 9.08 and a refraction index (n) of 1.424. For the ^{195}Pt chemical shifts, $[PtCl_4]^{2-}$ was selected as the reference compound (calculated at the same level of theory), which itself has an experimental chemical shift between 1600 and 1630 ppm compared to the primary reference complex ion $K_2[PtCl_6]$. Thus, the anisotropic shielding values from ORCA were further offset by an empirical value of +1600 ppm [$\delta = (\sigma_{ref} - 1600) - \sigma$].[60] Time-dependent DFT computations (TD-DFT) were run to obtain UV−vis spectra for the various structures at the same level of theory as geometry optimizations. Simulated UV−vis spectra were plotted with a Gaussian line shape and a line width of 8 nm.

■ ASSOCIATED CONTENT

Supporting Information

The Supporting Information is available free of charge at https://pubs.acs.org/doi/10.1021/acs.inorgchem.3c02869.

NMR spectra and ESI-MS data for all synthesized materials; coordinates for computationally minimized structures; and calculated UV−vis absorbance spectra (PDF)

■ AUTHOR INFORMATION

Corresponding Authors

Karin J. Young − *Department of Chemistry, Centre College, Danville, Kentucky 40422, United States;* orcid.org/0000-0003-3626-1854; Email: karin.young@centre.edu

Timothy P. Brewster − *Department of Chemistry, The University of Memphis, Memphis, Tennessee 38152, United States;* orcid.org/0000-0002-7654-4106; Email: tbrwster@memphis.edu

Authors

Natalie S. Taylor − *Department of Chemistry, The University of Memphis, Memphis, Tennessee 38152, United States*

Maxwell T. Gordinier − *Department of Chemistry, Centre College, Danville, Kentucky 40422, United States*

Tejaskumar Suhagia − *Department of Chemistry, The University of Memphis, Memphis, Tennessee 38152, United States*

Danna D. Pinto − *Department of Chemistry, The University of Memphis, Memphis, Tennessee 38152, United States*

Demetrius D. Cherry − *Department of Chemistry, Centre College, Danville, Kentucky 40422, United States*

Dominic S. Verry − *Department of Chemistry, Centre College, Danville, Kentucky 40422, United States*

Lindsey N. Baker − *Department of Chemistry, The University of Memphis, Memphis, Tennessee 38152, United States*

Nathan J. DeYonker − *Department of Chemistry, The University of Memphis, Memphis, Tennessee 38152, United States;* orcid.org/0000-0003-0435-2006

Complete contact information is available at: https://pubs.acs.org/10.1021/acs.inorgchem.3c02869

Author Contributions

The manuscript was written through contributions of all authors. All authors have given approval to the final version of the manuscript.

Funding

This work was supported, in part, by a grant from The University of Memphis College of Arts and Sciences Research Grant Fund (T.P.B.). This support does not necessarily imply endorsement by the University of research conclusions. N.S.T. thanks the University of Memphis for a Carnegie R1 Predoctoral Fellowship and a First-Generation Doctoral Fellowship. N.J.D. and T.S. were supported by the National Science Foundation (CAREER) BIO-1846408. Computational work was performed using resources at the University of Memphis High-Performance Computing Facility and the Computational Research on Materials Institute at the University of Memphis (CROMIUM). NMR data was obtained on an instrument acquired via NSF-MRI Grant No. CHE-1531466.

Notes

The authors declare no competing financial interest.

■ ACKNOWLEDGMENTS

The authors thank Mr. Drake Williams for his assistance in the collection of high-resolution mass spectra for newly synthesized materials and Dr. Alexander Erickson for his assistance with elemental analysis. The authors also thank Professor Dr. Alexander Auer (Max Planck Institute for Coal Research) for his help with ORCA computations.

■ REFERENCES

(1) Boor, J., Jr. *Ziegler-Natta Catalysts Polymerizations*, 1st ed.; Academic Press.
(2) Ittel, S. D.; Johnson, L. K.; Brookhart, M. Late-Metal Catalysts for Ethylene Homo- and Copolymerization. *Chem. Rev.* **2000**, *100* (4), 1169−1204.
(3) Chen, C. Designing Catalysts for Olefin Polymerization and Copolymerization: Beyond Electronic and Steric Tuning. *Nat. Rev. Chem.* **2018**, *2* (5), 6−14.
(4) Chen, J.; Gao, Y.; Marks, T. J. Early Transition Metal Catalysis for Olefin−Polar Monomer Copolymerization. *Angew. Chem., Int. Ed.* **2020**, *59* (35), 14726−14735.
(5) Jung, J.; Yasuda, H.; Nozaki, K. Copolymerization of Nonpolar Olefins and Allyl Acetate Using Nickel Catalysts Bearing a Methylene-Bridged Bisphosphine Monoxide Ligand. *Macromolecules* **2020**, *53* (7), 2547−2556.
(6) Drent, E.; van Dijk, R.; van Ginkel, R.; van Oort, B.; Pugh, R. I. Palladium Catalysed Copolymerisation of Ethene with Alkylacrylates: Polar Comonomer Built into the Linear Polymer Chain. *Chem. Commun.* **2002**, *7*, 744−745.
(7) Chen, S.-Y.; Pan, R.-C.; Chen, M.; Liu, Y.; Chen, C.; Lu, X.-B. Synthesis of Nonalternating Polyketones Using Cationic Diphosphazane Monoxide-Palladium Complexes. *J. Am. Chem. Soc.* **2021**, *143* (28), 10743−10750.
(8) Johnson, L. K.; Killian, C. M.; Brookhart, M. New Pd(II)- and Ni(II)-Based Catalysts for Polymerization of Ethylene and.Alpha.-Olefins. *J. Am. Chem. Soc.* **1995**, *117* (23), 6414−6415.
(9) Johnson, L. K.; Mecking, S.; Brookhart, M. Copolymerization of Ethylene and Propylene with Functionalized Vinyl Monomers by Palladium(II) Catalysts. *J. Am. Chem. Soc.* **1996**, *118* (1), 267−268.
(10) Konishi, Y.; Tao, W.; Yasuda, H.; Ito, S.; Oishi, Y.; Ohtaki, H.; Tanna, A.; Tayano, T.; Nozaki, K. Nickel-Catalyzed Propylene/Polar Monomer Copolymerization. *ACS Macro Lett.* **2018**, *7* (2), 213−217.
(11) Chen, Z.; Liu, W.; Daugulis, O.; Brookhart, M. Mechanistic Studies of Pd(II)-Catalyzed Copolymerization of Ethylene and Vinylalkoxysilanes: Evidence for a β-Silyl Elimination Chain Transfer Mechanism. *J. Am. Chem. Soc.* **2016**, *138* (49), 16120−16129.
(12) Wei, J.; Shen, Z.; Filatov, A. S.; Liu, Q.; Jordan, R. F. Self-Assembled Cage Structures and Ethylene Polymerization Behavior of Palladium Alkyl Complexes That Contain Phosphine-Bis(Arenesulfonate) Ligands. *Organometallics* **2016**, *35* (20), 3557−3568.
(13) Zhai, F.; Solomon, J. B.; Jordan, R. F. Copolymerization of Ethylene with Acrylate Monomers by Amide-Functionalized α-Diimine Pd Catalysts. *Organometallics* **2017**, *36* (9), 1873−1879.
(14) Contrella, N. D.; Sampson, J. R.; Jordan, R. F. Copolymerization of Ethylene and Methyl Acrylate by Cationic Palladium Catalysts That Contain Phosphine-Diethyl Phosphonate Ancillary Ligands. *Organometallics* **2014**, *33* (13), 3546−3555.
(15) Carrow, B. P.; Nozaki, K. Synthesis of Functional Polyolefins Using Cationic Bisphosphine Monoxide−Palladium Complexes. *J. Am. Chem. Soc.* **2012**, *134* (21), 8802−8805.
(16) Mitsushige, Y.; Yasuda, H.; Carrow, B. P.; Ito, S.; Kobayashi, M.; Tayano, T.; Watanabe, Y.; Okuno, Y.; Hayashi, S.; Kuroda, J.; Okumura, Y.; Nozaki, K. Methylene-Bridged Bisphosphine Monoxide Ligands for Palladium-Catalyzed Copolymerization of Ethylene and Polar Monomers. *ACS Macro Lett.* **2018**, *7* (3), 305−311.
(17) Chen, M.; Chen, C. A Versatile Ligand Platform for Palladium- and Nickel-Catalyzed Ethylene Copolymerization with Polar Monomers. *Angew. Chem., Int. Ed.* **2018**, *57* (12), 3094−3098.
(18) Zhao, M.; Chen, C. Accessing Multiple Catalytically Active States in Redox-Controlled Olefin Polymerization. *ACS Catal.* **2017**, *7* (11), 7490−7494.
(19) Peng, D.; Chen, C. Photoresponsive Palladium and Nickel Catalysts for Ethylene Polymerization and Copolymerization. *Angew. Chem., Int. Ed.* **2021**, *60* (41), 22195−22200.
(20) Tan, C.; Chen, C. Emerging Palladium and Nickel Catalysts for Copolymerization of Olefins with Polar Monomers. *Angew. Chem., Int. Ed.* **2019**, *58* (22), 7192−7200.
(21) Zhang, W.; Waddell, P. M.; Tiedemann, M. A.; Padilla, C. E.; Mei, J.; Chen, L.; Carrow, B. P. Electron-Rich Metal Cations Enable Synthesis of High Molecular Weight, Linear Functional Polyethylenes. *J. Am. Chem. Soc.* **2018**, *140* (28), 8841−8850.
(22) Cao, L.; Cai, Z.; Li, M. Phosphinobenzenamine Nickel Catalyzed Efficient Copolymerization of Methyl Acrylate with Ethylene and Norbornene. *Macromolecules* **2022**, *55* (9), 3513−3521.
(23) Carrow, B. P.; Nozaki, K. Transition-Metal-Catalyzed Functional Polyolefin Synthesis: Effecting Control through Chelating Ancillary Ligand Design and Mechanistic Insights. *Macromolecules* **2014**, *47* (8), 2541−2555.
(24) Luo, S.; Vela, J.; Lief, G. R.; Jordan, R. F. Copolymerization of Ethylene and Alkyl Vinyl Ethers by a (Phosphine- Sulfonate)PdMe Catalyst. *J. Am. Chem. Soc.* **2007**, *129* (29), 8946−8947.
(25) Tolman, C. A. Electron Donor-Acceptor Properties of Phosphorus Ligands. Substituent Additivity. *J. Am. Chem. Soc.* **1970**, *92* (10), 2953−2956.
(26) Perrin, L.; Clot, E.; Eisenstein, O.; Loch, J.; Crabtree, R. H. Computed Ligand Electronic Parameters from Quantum Chemistry and Their Relation to Tolman Parameters, Lever Parameters, and Hammett Constants. *Inorg. Chem.* **2001**, *40* (23), 5806−5811.
(27) Bartik, T.; Himmler, T.; Schulte, H.-G.; Seevogel, K. Substituenteneinflüsse Auf Die Basizität von Phosphorliganden in R3P-Ni(CO)3-Komplexen. *J. Organomet. Chem.* **1984**, *272* (1), 29−41.
(28) Brewster, T. P.; Nguyen, T. H.; Li, Z.; Eckenhoff, W. T.; Schley, N. D.; DeYonker, N. J. Synthesis and Characterization of Heterobimetallic Iridium−Aluminum and Rhodium−Aluminum Complexes. *Inorg. Chem.* **2018**, *57* (3), 1148−1157.
(29) Chianese, A. R.; Li, X.; Janzen, M. C.; Faller, J. W.; Crabtree, R. H. Rhodium and Iridium Complexes of N-Heterocyclic Carbenes via Transmetalation: Structure and Dynamics. *Orgranometallics* **2003**, *22* (8), 1663−1667.
(30) Bemowski, R. D.; Singh, A. K.; Bajorek, B. J.; DePorre, Y.; Odom, A. L. Effective Donor Abilities of E-t-Bu and EPh (E = O, S, Se, Te) to a High Valent Transition Metal. *Dalton Trans.* **2014**, *43* (32), 12299−12305.
(31) Fey, N.; Harvey, J. N.; Lloyd-Jones, G. C.; Murray, P.; Orpen, A. G.; Osborne, R.; Purdie, M. Computational Descriptors for Chelating P,P- and P,N-Donor Ligands1. *Organometallics* **2008**, *27* (7), 1372−1383.
(32) Jover, J.; Fey, N.; Harvey, J. N.; Lloyd-Jones, G. C.; Orpen, A. G.; Owen-Smith, G. J. J.; Murray, P.; Hose, D. R. J.; Osborne, R.; Purdie, M. Expansion of the Ligand Knowledge Base for Chelating P,P-Donor Ligands (LKB-PP). *Organometallics* **2012**, *31* (15), 5302−5306.
(33) Gensch, T.; dos Passos Gomes, G.; Friederich, P.; Peters, E.; Gaudin, T.; Pollice, R.; Jorner, K.; Nigam, A.; Lindner-D'Addario, M.; Sigman, M. S.; Aspuru-Guzik, A. A Comprehensive Discovery Platform for Organophosphorus Ligands for Catalysis. *J. Am. Chem. Soc.* **2022**, *144* (3), 1205−1217.
(34) Wucher, P.; Goldbach, V.; Mecking, S. Electronic Influences in Phosphinesulfonato Palladium(II) Polymerization Catalysts. *Organometallics* **2013**, *32* (16), 4516−4522.
(35) Ota, Y.; Ito, S.; Kuroda, J.; Okumura, Y.; Nozaki, K. Quantification of the Steric Influence of Alkylphosphine−Sulfonate Ligands on Polymerization, Leading to High-Molecular-Weight Copolymers of Ethylene and Polar Monomers. *J. Am. Chem. Soc.* **2014**, *136* (34), 11898−11901.

https://doi.org/10.1021/acs.inorgchem.3c02869
Inorg. Chem. 2024, 63, 2888−2898

(36) Akita, S.; Guo, J.-Y.; Seidel, F. W.; Sigman, M. S.; Nozaki, K. Statistical Analysis of Catalytic Performance in Ethylene/Methyl Acrylate Copolymerization Using Palladium/Phosphine-Sulfonate Catalysts. *Organometallics* **2022**, *41* (22), 3185−3196.
(37) Nakano, R.; Chung, L. W.; Watanabe, Y.; Okuno, Y.; Okumura, Y.; Ito, S.; Morokuma, K.; Nozaki, K. Elucidating the Key Role of Phosphine−Sulfonate Ligands in Palladium-Catalyzed Ethylene Polymerization: Effect of Ligand Structure on the Molecular Weight and Linearity of Polyethylene. *ACS Catal.* **2016**, *6* (9), 6101−6113.
(38) Chaudhury, N.; Puddephatt, R. J. Preparation and Electronic Spectra of Some Alkyl- and Aryl(2,2′-Bipyridine)Platinum(II) Complexes. *J. Organomet. Chem.* **1975**, *84* (1), 105−115.
(39) Jawad, J. K.; Puddephatt, R. J. Electronic and Steric Effects on the Rate of Oxidative Addition of Methyl Iodide to Diaryl(2,2′-Bipyridyl)Platinum(II) Complexes. *J. Chem. Soc., Dalton Trans.* **1977**, *15*, 1466−1469.
(40) Hollis, T. K.; Webster, C. E.; Zhang, M.; Dornshuld, E. V.; Dixet, V.; Camacho-Bunquin, J.; Delferro, M. *NHC Pincer Complex Donor Ability PtEP (Platinum (Pt) Electronic Parameter): A Donicity Scale Incorporating Strictly Meridional, Tridentate Ligands.*, American Chemical Society, 2018, Abstracts of Papers, 255th ACS National Meeting & Exposition, New Orleans, LA, INORG-496.
(41) Egan, T. J.; Koch, K. R.; Swan, P. L.; Clarkson, C.; Van Schalkwyk, D. A.; Smith, P. J. In Vitro Antimalarial Activity of a Series of Cationic 2,2′-Bipyridyl- and 1,10-Phenanthrolineplatinum(II) Benzoylthiourea Complexes. *J. Med. Chem.* **2004**, *47* (11), 2926−2934.
(42) Taft, R. W., Jr. Linear Free Energy Relationships from Rates of Esterification and Hydrolysis of Aliphatic and Ortho-Substituted Benzoate Esters. *J. Am. Chem. Soc.* **1952**, *74* (11), 2729−2732.
(43) Pangborn, A. B.; Giardello, M. A.; Grubbs, R. H.; Rosen, R. K.; Timmers, F. J. Safe and Convenient Procedure for Solvent Purification. *Organometallics* **1996**, *15* (5), 1518−1520.
(44) Baker, W. R.; Ryckman, D. M.; Cai, S.; Dimitroff, M.; Shang, X. Quinoline Antibacterial Compounds and Methods of Use Thereof. WO0218345A12002.
(45) Grushin, V. V. Synthesis of Hemilabile Phosphine−Phosphine Oxide Ligands via the Highly Selective Pd-Catalyzed Mono-Oxidation of Bidentate Phosphines: Scope, Limitations, and Mechanism. *Organometallics* **2001**, *20* (18), 3950−3961.
(46) Adamo, C.; Barone, V. Toward Reliable Density Functional Methods without Adjustable Parameters: The PBE0Model. *J. Chem. Phys.* **1999**, *110* (13), 6158−6170.
(47) Perdew, J. P.; Burke, K.; Ernzerhof, M. Generalized Gradient Approximation Made Simple. *Phys. Rev. Lett.* **1996**, *77* (18), 3865−3868.
(48) Grimme, S.; Ehrlich, S.; Goerigk, L. Effect of the Damping Function in Dispersion Corrected Density Functional Theory. *J. Comput. Chem.* **2011**, *32* (7), 1456−1465.
(49) Grimme, S.; Antony, J.; Ehrlich, S.; Krieg, H. A Consistent and Accurate Ab Initio Parametrization of Density Functional Dispersion Correction (DFT-D) for the 94 Elements H-Pu. *J. Chem. Phys.* **2010**, *132* (15), No. 154104.
(50) Neese, F. Software Update: The ORCA Program System—Version 5.0. *WIREs Comput. Mol. Sci.* **2022**, *12* (5), No. e1606.
(51) Weigend, F.; Ahlrichs, R. Balanced Basis Sets of Split Valence, Triple Zeta Valence and Quadruple Zeta Valence Quality for H to Rn: Design and Assessment of Accuracy. *Phys. Chem. Chem. Phys.* **2005**, *7* (18), 3297−3305.
(52) Rolfes, J. D.; Neese, F.; Pantazis, D. A. All-Electron Scalar Relativistic Basis Sets for the Elements Rb−Xe. *J. Comput. Chem.* **2020**, *41* (20), 1842−1849.
(53) van Lenthe, E.; Baerends, E. J.; Snijders, J. G. Relativistic Regular Two-component Hamiltonians. *J. Chem. Phys.* **1993**, *99* (6), 4597−4610.
(54) van Lenthe, E.; Ehlers, A.; Baerends, E.-J. Geometry Optimizations in the Zero Order Regular Approximation for Relativistic Effects. *J. Chem. Phys.* **1999**, *110* (18), 8943−8953.
(55) van Lenthe, E.; Baerends, E. J.; Snijders, J. G. Relativistic Total Energy Using Regular Approximations. *J. Chem. Phys.* **1994**, *101* (11), 9783−9792.
(56) Wolff, S. K.; Ziegler, T. Calculation of DFT-GIAO NMR Shifts with the Inclusion of Spin-Orbit Coupling. *J. Chem. Phys.* **1998**, *109* (3), 895−905.
(57) Schreckenbach, G.; Ziegler, T. Calculation of NMR Shielding Tensors Using Gauge-Including Atomic Orbitals and Modern Density Functional Theory. *J. Phys. Chem. A* **1995**, *99* (2), 606−611.
(58) Neese, F. An Improvement of the Resolution of the Identity Approximation for the Formation of the Coulomb Matrix. *J. Comput. Chem.* **2003**, *24* (14), 1740−1747.
(59) Barone, V.; Cossi, M. Quantum Calculation of Molecular Energies and Energy Gradients in Solution by a Conductor Solvent Model. *J. Phys. Chem. A* **1998**, *102* (11), 1995−2001.
(60) Tsipis, A. C.; Karapetsas, I. N. Accurate Prediction of 195Pt NMR Chemical Shifts for a Series of Pt(II) and Pt(IV) Antitumor Agents by a Non-Relativistic DFT Computational Protocol. *Dalton Trans.* **2014**, *43* (14), 5409−5426.

https://doi.org/10.1021/acs.inorgchem.3c02869
Inorg. Chem. 2024, 63, 2888−2898